Published in final edited form as:
Neurobiol Dis. 2011 March ; 41(3): 706–716. doi:10.1016/j.nbd.2010.12.008.

Adult neurogenesis and neurite outgrowth are impaired in *LRRK2* G2019S mice

B Winner[1,5], **HL Melrose**[2,5], **C Zhao**[1], **KM Hinkle**[2], **M Yue**[2], **C Kent**[2], **AT Braithwaite**[2], **S Ogholikhan**[2], **R Aigner**[3], **J Winkler**[3,6], **MJ Farrer**[2,4,6], and **FH Gage**[1,6]

[1]Laboratory of Genetics, The Salk Institute for Biological Studies, La Jolla, CA 92186, USA

[2]Department of Neuroscience, Mayo Clinic, Jacksonville, Florida 32224, USA

[3]Division of Molecular Neurology, University Hospital of Erlangen, Erlangen, Germany

[4]Department of Medical genetics, University of British Columbia, Vancouver, Canada

Abstract

The generation and maturation of adult neural stem/progenitor cells are impaired in many neurodegenerative diseases, among them Parkinson's disease (PD). In mammals, including humans, adult neurogenesis is a lifelong feature of cellular brain plasticity in the hippocampal dentate gyrus (DG) and in the subventricular zone (SVZ)/olfactory bulb system. Hyposmia, depression, and anxiety are early non-motor symptoms in PD. There are parallels between brain regions associated with non-motor symptoms in PD and neurogenic regions. In autosomal dominant PD, mutations in the leucine-rich repeat kinase 2 (*LRRK2*) gene are frequent. *LRRK2* homologs in non-vertebrate systems play an important role in chemotaxis, cell polarity, and neurite arborization.

We investigated adult neurogenesis and the neurite development of new neurons in the DG and SVZ/olfactory bulb system in bacterial artificial chromosome (BAC) human Lrrk2 G2019S transgenic mice. We report that mutant human Lrrk2 is highly expressed in the hippocampus in the DG and the SVZ of adult Lrrk2 G2019S mice. Proliferation of newly generated cells is significantly decreased and survival of newly generated neurons in the DG and olfactory bulb is also severely impaired. In addition, after stereotactic injection of a GFP retrovirus, newly generated neurons in the DG of Lrrk2 G2019S mice exhibited reduced dendritic arborization and fewer spines. This loss in mature, developed spines might point towards a decrease in synaptic connectivity. Interestingly, physical activity partially reverses the decrease in neuroblasts observed in Lrrk2 G2010S mice. These data further support a role for Lrrk2 in neuronal morphogenesis and provide new insights into the role of Lrrk2 in adult neurogenesis.

Keywords

neural progenitor cells; neurogenesis; Parkinson's disease; dendrites; spines; *LRRK2*

Corresponding authors: Fred H. Gage, Laboratory of Genetics, The Salk Institute for Biological Studies, 10010, North Torrey Pines Road, La Jolla, CA 92186, USA, gage@salk.edu, Beate Winner, beate.winner@med.uni-erlangen.de.
[5,6]contributed equally
present address: Junior Research Group III, Interdisciplinary Center for Clinical Research, Nikolaus-Fiebiger Center for Molecular Medicine, Friedrich-Alexander-Universität Erlangen-Nürnberg, Glücksstr. 6, 91054 Erlangen, Germany

Introduction

Mutations in *leucine-rich repeat kinase 2* (*LRRK2*) predispose carriers to Parkinson's disease (PD; (Zimprich et al 2004a); (Mata et al 2006). Lrrk2 G2019S is found in more than 30% of patients of certain ethnicities and has the highest genotype- and population-attributable risk (Hulihan et al 2008); (Healy et al 2008).

LRRK2 is comprised of 51 exons that encode 2,527 amino acids and has a molecular mass of 286kDa. Lrrk2 is a large, multi-domain protein kinase and consists of an ankyrin repeat region, leucine-rich repeats, a Roc GTPase domain, and a C terminal of Roc (COR) domain. In addition, a serine/threonine protein kinase domain with a high degree of homology with MAPKKK (mitogen-activated protein kinase kinase kinase, where the G2019S mutation is located) and a WD40 domain are present (Mata et al 2006); (Zimprich et al 2004b). While Lrrk2 transgenic models are yet to recapitulate human PD neuropathology in aspects such as increased cell death of dopaminergic neurons or Lewy bodies, subtle phenotypes including impaired regulation of neurite growth and arborization have been reported. In non-vertebrate systems a role of *LRRK2 homologs* for chemotaxis, polarization, and regulation of axonal-dendritic polarity of synaptic vesicle proteins was described (van Egmond et al 2008, Sakaguchi-Nakashima et al 2007). In primary neuronal cultures, *in utero* transfection or AAV2 viral injection, mutant Lrrk2 slows axonal outgrowth and reduces neurite length and branching, whereas silencing of *LRRK2* leads to the opposite effects (Li et al 2009; MacLeod et al 2006; Plowey et al 2008).

In humans and mice, Lrrk2 is highly expressed in the hippocampus and subventricular zone (SVZ) and colocalizes with the migrating neuroblast marker PSA-NCAM (Melrose et al 2007). The hippocampal dentate gyrus (DG) and SVZ/olfactory bulb system are the physiological areas of neurogenesis in the adult brain (Altman & Das 1965; Curtis et al 2007; Eriksson et al 1998). In PD and transgenic SNCA mouse models of parkinsonism, the proliferation of dividing cells is impaired in the DG and SVZ/olfactory bulb system (Crews et al 2008; Hoglinger et al 2004; Winner et al 2004). PD affects multiple neurotransmitter systems and includes a variety of non-motor symptoms (Langston 2006). Frequently observed early symptoms in PD include hyposmia, anxiety, anhedonia, and depression (Tolosa & Poewe 2009). These symptoms are linked to neuropathological alterations in the olfactory and limbic system, including the olfactory bulb and the hippocampus (Rodriguez-Oroz et al 2009).

In this study, we take advantage of the hippocampal and SVZ transgene expression in G2019S Lrrk2 mice to study the impact of mutated Lrrk2 on newly generated neurons in the adult brain. With the benefit of inherent Lrrk2 expression, we examine the impact of aberrant human Lrrk2 on adult neurogenesis. We determine neurite outgrowth, and spine numbers in newly generated neurons in the hippocampal DG *in vivo* and test whether physical activity impacts this system.

Methods

Animals

All animal procedures were approved by the Mayo Clinic Institutional Animal Care and Use Committee (IACUC) and were in accordance with the National Institute of Health Guide for the Care and Use of Laboratory Animals (NIH Publications No. 80-23) revised 1996. All mice were kept in a normal light/dark cycle (12 hours light/ 12 hours dark) and had free access to food and water.

Generation of BAC transgenic mice

A Bacterial Artificial Chromosome (BAC) (RP-11 568G5) containing the entire human wild-type *LRRK2* gene and regulatory sequences was identified using the Celera Database and purchased from the Children's Hospital Oakland Research Institute (Oakland, CA). Recombination-based BAC mutagenesis was performed on RP-11 568G5 to generate mutant a G2019S BAC clone, which was sequenced to confirm the mutation. Following confirmation of integrity, purified BAC DNA was injected into FVB/N (Taconic, Germantown, NY) fertilized oocytes and transplanted into pseudo-pregnant ICR (Harlan, Indianapolis, IN) female mice. Subsequent offspring were genotyped by polymerase chain reaction (PCR) using two sets of primers designed within the vector arms and the human 5' and 3' insert, to identify founders. Transgenic founders were bred to FVB mice and transgenic F1 offspring were analyzed for gene and protein expression. A colony was expanded for the G2019S line with the highest expression level. General characteristics of these mice are recently described elsewhere (Melrose et al 2010).

Real time quantitative reverse transcriptase polymerase chain reaction (qRT-PCR)

Mice were euthanized by cervical dislocation and brains were carefully separated into different regions (olfactory bulb, hippocampus, striatum, cortex, mid-brain, brainstem, cerebellum) and frozen on dry ice. RNA was isolated using TRIzol® (Invitrogen, Carlsbad, CA,) according to manufacturer's instructions. cDNA was synthesized using Superscript II (Invitrogen). Real time PCR assays were performed in triplicate on a 384 well plate using an ABI 7900 detection system to assess the relative level of human *LRRK2* mRNA using TaqMan® probe Hs00417273 ml specific for human *LRRK2* (ABI, Foster City, CA, USA). Murine GAPDH (Mm99999915 ml) was used as the endogenous reference gene.

In situ hybridization

Cartridge purified oligonucleotides were synthesized by Sigma Genosys (St Louis, MO, USA). Human *LRRK2* was detected with an oligonucleotide 5'TTTAAGGCTTCCTAGCTGTGCTGTCATCATGACTCTG'3 designed to human exon 41. 100 ng of oligonucleotide was 3' end labeled with ^{33}P α-dATP (Perkin Elmer, Boston, MA, USA) using Terminal Transferase (Roche, Indianapolis, IN, USA). Labeled oligonucleotides were purified using Nick columns (Amersham, Piscataway, NJ, USA) and the specific activity checked to ensure a minimum of 1×10^8 cpm/μg.

15-μm coronal frozen cryostat sections were fixed in cold 4% paraformaldehyde in Sörensen's phosphate buffer, dehydrated in ascending alcohols and incubated at 37°C overnight in hybridization buffer (4× Standard sodium citrate, 50% (w/v) formamide, 10% (w/v) dextran sulfate, 200mg/μl Herring Sperm DNA) containing ^{33}P α-dATP labeled oligonucleotides. Competition hybridizations performed in the presence of excess unlabeled probe served as an additional control for each oligonucleotide. Slides were stringently washed three times in 1× SSC at 55°C and exposed to Kodak MS high-resolution film for 10–14 days.

Antibodies

Affinity purified rabbit polyclonal antibody PA0362 (C-terminal amino acid residues 2507–2527) was raised to synthetic human Lrrk2 peptides (Melrose et al 2007). Primary antibodies were as follows: rat α-5-bromo-2-deoxyuridine (BrdU) 1:500 (Oxford Biotechnology, Oxford, UK); mouse α-NeuN 1:500, rabbit α-Tyrosine hydroxylase (TH, all Chemicon, Temecula, CA, USA), and goat α-doublecortin (DCX) 1:500, (Santa Cruz Biotechnology, Santa Cruz, CA, USA). Secondary antibodies for immunofluorescence were donkey anti-goat, -mouse, -rabbit or -rat conjugated with fluorescein (FITC), rhodamine X

(RHOX), CY5 or biotin 1:500 (Jackson Immuno Research, West Grove, PA, USA). For immunohistochemistry, donkey anti-mouse, -rabbit or -goat biotinylated 1:500 (Jackson Immuno Research, West Grove, PA, USA) and avidin-biotin-peroxidase complex 1:100 (Vectastain Elite, Vector Laboratories, Burlingame, CA, USA) were used.

Lrrk2 Immunoblotting

Tissue was homogenized in 5 volumes [V/m) of homogenization buffer (50 mM Na_2PO_4, 10 mM $Na_4P_2O_7.10H_2O$, 20 mM NaF, 2 mM EGTA, 2 mM EDTA, 2 mM $Na_3VO_4$2 mM DTT), protease inhibitor cocktail (Sigma, St. Louis, MO) and phosphatase inhibitor cocktails I and II (Sigma). Samples were centrifuged at 12,000×*g* for 5 minutes at 4°C. The supernatant was collected and assayed for protein concentration (Pierce Biotechnology, Inc/ ThermoFisher Scientific Rockford, IL). Samples were denatured in sodium dodecyl sulphate sample buffer before being resolved on a 3–8% Tris-acetate gel (Invitrogen). Blots were blocked in 5% non-fat milk in Tris buffered-saline-Tween and probed with primary antibody overnight at 4°C (PA0362 1:500). The blots were incubated with the appropriate conjugated secondary antibodies, and bands were visualized using enhanced chemiluminescence (Pierce Biotechnology).

Analysis of adult neurogenesis

Lrrk2 G2019S BAC mice were compared to non-transgenic (NT) littermate controls. The animals were four months old at the beginning of the experiment. For the proliferation study, G2019S mice and NT controls received a single injection of BrdU, (100 mg/kg), and the mice were perfused 24 hours after the injection (experimental design: Fig. 2A, n=5 per group). In an additional experiment, survival of newly generated neurons was studied. Here the mice received daily intraperitoneal injections of BrdU (50 mg/kg) for five consecutive days and were sacrificed one month after the BrdU injections (experimental design: Fig. 3A, n=5 per group).

Retrovirus-mediated labeling of new neurons in the mouse hippocampus

The murine Moloney leukemia virus-based retroviral vector CAG-GFP (a gift from Drs. Gerald Pao and Inder Verma, Salk Institute, La Jolla, CA) uses the backbone of pCLNCXv. 2; the compound promoter CAG expression drives the expression of GFP. The concentrated viral solution (10^8 pfu/ml) was prepared and stereotactically injected as described previously (Zhao et al 2006) into the DG at the following coordinates: AP: 2, ML: −1.6, DV −2.3/ 2.2 (from skull, n 5 per group for G2019S and NT control mice).

Running experiment

For a third set of experiments, G2019S mice and NT controls were exposed to a running wheel in their cages. The non-running (non-run) control groups were placed in same-size standard cages including the base of the running wheel (n=4 per group for NT and Lrrk2 G2019S). The running group (run) had free access to a running wheel in each cage (n=4 per group for NT and G2019S) for a total of six weeks. Physical appearance and time spent on the running wheel were checked daily, and all animals made use of the running wheels provided. All animals were sacrificed at four months.

Mice were deeply anesthetized with chloral hydrate and perfused transcardially with 4% paraformaldehyde in 100 mM phosphate buffer (PB), pH 7.4. The brains were removed, post-fixed in 4% paraformaldehyde/ PB for 24 hours, and processed as previously described (Winner et al., 2008b).

Immunohistochemistry and immunofluorescence—Free-floating sections were stained by applying primary antibodies in TBS/donkey serum overnight at 4°C and biotinylated secondary antibodies and avidin-biotin-peroxidase complex as previously described (Winner et al., 2008b). For detection of BrdU-labeled nuclei, the following DNA denaturation steps preceded the incubation with anti-BrdU antibody: two-hour incubation in 50% formamide/2×SSC (2×SSC: 0.3 M NaCl, 0.03 M sodium citrate) at 65°C, five-min rinse in 2×SSC, 30-min incubation in 2 M HCl at 37°C, and 10-min rinse in 0.1 M boric acid, pH 8.5. For immunofluorescence staining, free-floating sections for BrdU staining were treated to denature the DNA as described above. Afterwards the combination of antibodies was applied as described previously (Winner et al 2008a).

For Lrrk2 immunostaining, 15-μm thick frozen sections were briefly fixed in 10% buffered formalin. Following endogenous peroxidase blocking, sections were treated to block endogenous fluorescence by incubation with 0.1% Sudan black in 70% ethanol for 10 minutes. After washing, sections were blocked for 30 minutes in TNB blocking buffer (0.1M Tris-HCL, pH 7.5, 0.15M NaCl, 0.5% blocking reagent), reconstituted from reagents provided in a Renaissance® Tyramide Signal Amplification (TSA)™ Biotin or Plus Fluorescence System kits (PerkinElmer). Sections were then incubated with PA0362 antibody (Lee et al 2010; Melrose et al 2007) diluted 1:100 in TNB blocking buffer for 48 hours at room temperature. Secondary antibody was Biotin-SP-conjugated AffiniPure Donkey Anti-Rabbit IgG (H+L) (Jackson ImmunoResearch) diluted 1:500 in TNB blocking buffer at room temperature (RT) for 30 min. TSA amplification was then performed according to manufacturer's instructions. Subsequently, sections were incubated with strepavidin-conjugated Cy-2 (Jackson ImmunoResearch) diluted 1:100 in PBS for 30 min at RT.

Counting procedures

For quantification, a systematic, random counting procedure, similar to the optical dissector (Gundersen et al 1988; Williams & Rakic 1988), was used as previously described (Winner et al 2008b), Stereoinvestigator, MicroBrightField, Colchester, VT, USA). Cells were counted exhaustively in the DG, SVZ and glomerular layer of the olfactory bulb and by using using a semiautomatic stereology system for the granule cell layer of the olfactory bulb. Briefly, in the granule cell layer of the olfactory bulb, BrdU-positive cells were counted within a 30 × 30 μm counting frame, which was spaced in a 300 × 300 μm counting grid. Positive profiles that intersected the uppermost focal plane (exclusion plane) or the lateral exclusion boundaries of the counting frame were not counted. The total counts of positive profiles were multiplied by the ratio of reference volume to sampling volume to obtain the estimated number of positive cells.

Confocal images were generated by using a confocal laser microscope (Leica TCS-NT, Bensheim, Germany) equipped with a 40 × PL APO oil objective (1.25 numeric aperture) and a pinhole setting that corresponded to a focal plane of 2 μm, as described previously (Winner et al., 2008). On average, 40 BrdU-positive cells were analyzed in each animal and each region for neuronal differentiation.

Dendritic growth of GFP-positive neurons—For dendritic growth analysis, z-series at 1.5-μm intervals were acquired with a Bio-Rad Radiance 2100 confocal system (Hercules, CA, USA). Two-dimensional maximum intensity projections of each z-series were created with the Confocal Assistance Program (Bio-Rad) in the BMP (bitmap) format, and the files were then imported into IGL Trace to measure dendritic length. The number of branching points/cell was counted manually from the same images. Eight to 10 cells per mouse (four mice per group) were analyzed.

Spine density and classification of mushroom spines—Images of GFP-labeled dendritic processes at the outer molecular layer were acquired at 0.5-μm intervals with the Bio-Rad R2100 confocal system with a plan apochromatic 60× oil lens [numerical aperture (NA), 1.4; Nikon] and a digital zoom of 5. The Bio-Rad image files were subjected to five iterations of deconvolution with the AutoDeblur program (AutoQuant, Troy, NY). Maximum intensity projections of z-series were created with the Confocal Assistance Program in BMP format, and the files were then imported into IGL Trace. The length of each dendritic segment was determined by tracing the center of the dendritic shaft, and the number of spines was counted manually from the two-dimensional projections. The linear spine density was calculated by dividing the total number of spines by the length of the dendritic segment. Classification of mushroom spines was performed as described previously (Zhao et al 2006). Briefly, major and minor axes of each spine head were identified. A spine was considered of mushroom type if the average estimated area from three measurements was 0.4 μm^2. For the final quantification, 25 or more dendritic segments from four mice per group were used. Confocal imaging and data quantification were performed blinded to the experimental conditions. The data are expressed as mean values ± standard deviation (SD). One-way analysis of variance (ANOVA) followed by Bonferroni multiple comparison test or student-t test was used (Prism Graph Pad Software, San Diego, Ca, USA). The significance level was set at $p < 0.05$.

Results

Human G2019S *Lrrk2* is highly expressed in regions of adult neurogenesis

Regional expression of transgenic *LRRK2* mRNA was assessed with a human-specific Taqman probe and revealed that the highest transgene expression in adult G2019S mice occurred in the hippocampal formation (Fig. 1A). Finer anatomical mapping using *in situ* hybridization with a *LRRK2* human-specific probe confirmed that high expression was found in the *Cornu Ammonis* fields and, importantly, in the DG (Fig. 1B). Consistent with mRNA results, immunoblotting with a Lrrk2 specific antibody, PA0362, revealed that Lrrk2 protein levels were robust in the hippocampus (Fig 1C), in agreement with the estimated 14-fold expression over endogenous levels previously reported for the hippocampus in this line (Melrose et al 2010). Expression of murine Lrrk2 in the SVZ was described in detail previously (Melrose et al 2007). While we are unable to determine the exact level of human transgenic over-expression in the SVZ by Western blotting, expression analysis in hemi-brains from transgenic mice previously revealed an overall 3-fold expression of transgenic Lrrk2 protein versus endogenous Lrrk2 (Melrose et al 2010). Immunofluorescence with the Lrrk2 antibody revealed robust Lrrk2 expression in chains of neuroblasts in both NT and G2019S mice (Fig. 2J–M).

Proliferation is markedly reduced in G2019S transgenic mice

As Lrrk2 is highly expressed in the adult DG and SVZ, we sought to ascertain whether this expression has an impact on cell proliferation. We analyzed the effect of Lrrk2 G2019S overexpression on newly generated cells in the hippocampal DG and SVZ 24 hours after a single injection of BrdU (Fig. 2A). We compared proliferation in G2019S versus NT littermate controls. Unbiased stereological counting methods were applied to estimate the number of BrdU-labeled cells. A significant decrease in BrdU-positive cells was detected in G2019S mice compared to NTs, as evidenced by a ~54% ($p<0.01$) decrease in proliferation in the DG (Fig. 2B, C) and in the SVZ (~36% decrease, $p<0.05$, Fig. 2D–F). The rostral migratory stream (RMS) appeared thinner in the Lrrk2 G2019S mice, with less BrdU-positive cells within this structure (Fig. 2G–I).

Survival of new neurons in the olfactory bulb is significantly decreased in G2019S transgenic mice

To investigate the survival of newly generated neurons, four-month-old G2019S mice and NT littermates received daily intraperitoneal injections of BrdU for five consecutive days and were sacrificed 30 days later (Fig. 3A). A significant decrease in numbers of newly generated neurons was present in the granule cell layer of the olfactory bulb (41% decrease compared to NT, $p<0.0001$, Fig. 3B–E) and the glomerular layer (73% decrease, $p<0.0001$, Fig. 3B, F–I). The ratio of neuronal (NeuN-positive) profiles among the BrdU-positive cells was not significantly altered; neurons represented the majority of newly generated cells, with 94% (NT) and 96% (G2019S) in the olfactory bulb granule cell layer and 81% (NT) and 74% (G2019S) in the glomerular layer. Moreover, the TH-positive neurons were significantly decreased in the glomerular layer of the olfactory bulb, where a 72% decrease of TH-positive cells was detected (Fig. 3J–M, $p<0.0001$). The ratio of dopaminergic differentiation was not significantly different between both groups [18% (NT) and 17% (G2019S) of all BrdU-positive cells].

Survival of new neurons in the DG is significantly decreased in G2019S transgenic mice

The number of BrdU-positive cells was reduced significantly in the DG of G2019S mice (73% decrease, $p=0.0002$) compared to the NT group (Fig. 4B). Adult neurogenesis was further studied by determining the fate of BrdU-labeled cells. The total number of newly generated neurons (BrdU/NeuN) was significantly reduced in the G2019S group (77% decrease, $p<0.001$, Fig. 4C, D). The percentages of neuronal differentiation of BrdU-positive cells did not differ significantly between NT (69%) and G2019S mice (64%). DG volumes were unchanged between transgenics and controls (0.1 mm^3 in both groups).

Dendrite length and branching points in new neurons are reduced in G2019S mice

To further analyze the dendritic morphology of newly generated neurons in G2019S mice compared to NT controls, we delivered concentrated GFP retrovirus ($1\times^8$ transduction units/ml) into the DG of three-month-old G2019S transgenic and NT mice. Brains were harvested one month after the retroviral injection (Fig. 5A). At this time point, the dendrites of newborn granule cells in control animals showed a highly polarized morphology. Retrovirus-mediated gene transfer allows the study of the morphological details of neurite outgrowth in new neurons (Zhao et al 2006). They had an elaborate dendritic arbor with abundant spines extending into the molecular layer (Fig. 5B), and the axons had reached their target area, CA3 (van Praag et al 2002;Zhao et al 2006). However, in the G2019S mice, less dendritic arborization and shorter dendrite lengths were observed (Fig. 5B). We measured dendrite length and branching points and found a 60% decrease in dendrite length in the G2019S group (Fig. 5C, $p<0.0001$). In addition, the arborization was severely impaired in these animals, with a decrease of 66% in branching points ($p<0.0001$, Fig. 5D).

Spine density and mushroom spines are decreased in G2019S mice

Mature granule neurons receive most of their synaptic inputs from the entorhinal cortex through dendritic spines. Therefore, the number and shape of the dendritic spines are indicative of the connectivity of these newly generated cells. We asked whether spine density and development were also affected in the G2019S transgenic mice. The time point analyzed reflects a stage of late spine development (Fig. 6a; van Praag et al 2002). A significant difference was found in the G2019S group, with a 64% decrease in spine density ($p<0.001$, Fig. 6B, C). Spines have been categorized into different types on the basis of their morphology, which also reflects their maturation stage: mushroom, thin, stubby, and filopodia. Mushroom spines are more abundant in mature neurons, whereas thin, stubby and filopodia are immature developing stages (Nimchinsky et al 2002,Sala 2002). Interestingly,

the number of mushroom spines was decreased in G2019S mice, indicating that, at this time point, mature, developed spines are less frequent in G2019S mice (decrease of 53%, $p<0.001$, Fig. 6D).

Running increases the generation of new neurons in *Lrrk2* G2019S mice

The rate of neurogenesis in the mammalian brain is not constant but can be influenced by numerous factors, among them enhancement by voluntary physical activity (van Praag et al 1999b). Enhanced physical activity subsequent to the introduction of a running wheel doubles proliferation in the DG as compared to what is observed in mice housed in standard conditions (van Praag et al 1999b). Moreover, voluntary physical activity increases the relative survival of the newly generated cells as well as the percentage of neuronal differentiation (van Praag et al 1999a). DCX is a marker used to assess and quantify changes occurring in the rate of neurogenesis in the DG following enhanced physical activity (Couillard-Despres et al 2005). When comparing non-running NT and G2019S mice (Fig. 7A), the decrease in neurogenesis reported above for BrdU/NeuN cell numbers was also reflected in a decrease in numbers of DCX-expressing neuroblasts (decrease of 71% in G2019S, $p<0.001$, Fig. 7B, C). Compared to NT non-running mice, NT running mice showed a significant increase in numbers of DCX-positive cells as a result of the increased physical activity (34% increase, $p<0.05$). This effect is confirmed between different strains of mice (Kempermann et al 2006; van Praag et al 1999b). Interestingly, there is also a significant increase in numbers of DCX-positive cells in the running G2019S group, indicating that the decreased numbers of DCX-labeled cells in the DG of non-running Lrrk2 G2019S animals could be partially reversed by physical activity (nearly 3-fold increase compared to Lrrk2 G2019S non-running group) and not statistically different from NT non-runners. This finding suggests that increased physical activity is capable of partially reversing the decrease in neurogenesis induced by Lrrk2 G2019S overexpression.

Discussion

We have used a mouse model that expresses a high level of human Lrrk2 in regions of adult neurogenesis and endogenous Lrrk2 expression. We reported a significant decrease in SVZ/olfactory bulb and hippocampal adult neurogenesis in Lrrk2 G2019S transgenic mice, both at the level of proliferation and survival of newly generated cells. Moreover, impaired adult neurogenesis was accompanied by structural alterations of the newly generated cells in the DG, with decreases in neurite length and in spine numbers. Interestingly, the reduced neurogenesis in G2019S transgenic mice could be partly reversed by physical activity.

Our study reports a significant decrease in olfactory bulb adult neurogenesis. In particular, a significant decrease in proliferation in the SVZ results in fewer new granule cell neurons and fewer dopaminergic neurons in the glomerular layer. As levels of Lrrk2 are relatively high in the SVZ, we speculate that a cell-autonomous effect in the neural cells might be the reason for the decrease in olfactory neurogenesis. Alternatively, decreased dopaminergic neurotransmission could be an additional factor that could potentially contribute to reduced proliferation. Decreased extracellular striatal dopamine levels were reported in these animals (Melrose et al 2010) and decreased SVZ proliferation was also described previously for 6-OHDA lesions (Hoglinger et al 2004), (Winner et al 2006).

Newly generated olfactory interneurons undergo different experience-dependent synaptic modifications and provide a possible substrate for adult neurogenesis-dependent olfactory learning (Nissant et al 2009). How these affect olfaction in this animal model will be investigated by detailed olfactory testing in the future Olfactory dysfunction, among them odor identification, detection and discrimination of symptomatic Lrrk2 carriers varies

between 50% to more than 80% (Healy et al 2008; Khan et al 2005; Silveira-Moriyama et al 2008).

The decrease in proliferation in the DG might partly explain reduced numbers of newly generated neurons. In our model, similar to previous reports, LRRK2 is strongly expressed postnatally (West et al 2007), which might explain, that the decrease in neurogenesis does not have an effect on DG volume. However, the altered morphology of newly generated neurons, with shorter dendritic length and less branching, suggests that, even if cells survive the period of proliferation, integration may be impaired in Lrrk2 mice. Reduced neurite outgrowth has been described for Lrrk2 in primary neuronal cultures, embryonic brains and following AAV2 injection (MacLeod et al 2006). Besides a severe decrease in dendrite length, we observed a decrease in spines and, in particular, in mature mushroom spines.

Ezrin/Radixin/Moesin (ERM) proteins are physiologically expressed in neurogenic regions in the adult (Persson et al 2010). Interestingly, a recent paper reports that phosphorylation of ERM proteins by Lrrk2 promotes the rearrangement of actin cytoskeleton in neuronal morphogenesis (Parisiadou et al 2009). In G2019S primary hippocampal cultures derived from inducible BAC mice, an increase in ERM phosphorylation was accompanied by an increase in filopodia (Parisiadou et al 2009). While a more detailed analysis is required, we speculate that aberrant Lrrk2 may interfere with the maturation of filopodia into spines. Other models of parkinsonism (e.g. human wild-type overexpression α-synuclein transgenic animals) also present with impaired neurite development of newly generated neurons. Here changes in DCX-neuroblast morphology were noted. Specifically, the DCX-positive cells in a-synuclein transgenic animals had shorter and less elaborated processes (Winner et al 2004).

In asymptomatic *LRRK2* mutation carriers, a smaller hippocampal gray matter volume was recently described (Reetz et al 2010). It is intriguing that DG neurogenesis is involved in regulation of emotion and might have an impact on the effectiveness of antidepressants (Sahay & Hen 2007; Santarelli et al 2003). G2019S mice display anxiety-like behaviors in the open field test compared with NT mice, as evidenced by increased path length and thigmotaxis (Melrose et al 2010). Unfortunately, the visual impairment of the G2019S animals on FVB/N background (FVB/N mice are homozygous for the retinal degeneration gene) prevented testing with DG-dependent tasks for spatial orientation. Detailed DG-dependent behavioral studies will be conducted in future studies using a different genetic background.

Our findings of decreased adult neurogenesis have parallels with Huntington's disease (HD), where the non-striatal pathology, especially that of the hippocampus, is suspected to mediate aspects of affective and cognitive deficits in HD patients (Rosas et al 2003). In addition, environmental enrichment improves motor and cognitive deficits in HD transgenic mice models (van Dellen et al 2000). Neural progenitor cell proliferation, survival and structure are abnormal in the DG of mice transgenic for the human HD gene (reviewed in (Clelland et al 2008), an effect that can be partially restored by environmental enrichment (Lazic et al 2006; Spires et al 2004) but not by running (Kohl et al 2007). However, physical activity does causes a robust increase in neurogenesis in the DG of the hippocampus in non-diseased (van Praag et al 1999b) and irradiated (Naylor et al 2008) brains and a beneficial effect of running on cognition has been speculated to be in part attributable to enhanced hippocampal neurogenesis. In Lrrk2 transgenic mice, the reduction in neurogenesis is partly reversed by physical activity. The running recovery difference here between the HD mice and the Lrrk2 mice is likely due to the underlying mechanisms (protein aggregation versus defective signaling) impacting on neurogenesis. In mice and humans, exercise improves mood and cognition (Babyak et al 2000; Suominen-Troyer et al 1986) and delays the onset of

neurodegenerative diseases, among them PD (Tillerson et al 2003). The mechanisms behind the beneficial effects of exercise on neurogenesis are not yet understood however several neurotrophic factors - among them brain derived neurotrophic factor (BDNF), vascular endothelial growth factor (VEGF), and TrkB tyrosine kinase (TrkB) – are increased by physical activity (Fabel et al 2003; Marais et al 2009) and some of them are able to reverse synapse loss in Alzheimer's disease models (Nagahara et al 2009). Physical activity can also activate kinase signaling pathways that are associated with neurogenesis including the mitogen activated kinase signaling (MAPK) and phosphatidylinositol 3-kinase (PI3K) pathways (Cotman et al 2007). Furthermore, inhibition of the PI3K-Akt signaling pathway blocks exercise mediated enhancement of adult neurogenesis (Bruel-Jungerman et al 2009). While the pathways involved in Lrrk2 kinase signaling are yet to be fully elucidated, several lines of evidence link Lrrk2 to MAPK signaling cascades (Carballo-Carbajal et al 2010; Gloeckner et al 2009; Hsu et al 2010; Liou et al 2008; Plowey et al 2008).With the caveat that signaling mechanisms involved in recovery of neurogenesis are not necessarily the same as those impacted by the mutation, our data may go some way to suggest that exercise induced signaling may at least partially be able compensate for aberrant Lrrk2 activity caused by the G2019S mutation.

Recently, new pro-neurogenic and neuroprotective agents were found to impede neuron death in the DG and preserve cognitive capacity (Pieper et al 2010). Transgenic models for neurodegenerative diseases, such as the one we describe here, will serve as useful tools for therapeutic evaluation of these drugs.

Our findings expand previous observations of Lrrk2 interference with process outgrowth to an adult *in vivo* model (MacLeod et al 2006; Plowey et al 2008; Wang et al 2008). In the current model, modulation of neurite outgrowth and neurogenesis of newly generated neurons may provide an early and constitutive assay for studying the neuronal dysfunction associated with Lrrk2 activity.

Acknowledgments

The authors would like to thank Ralf Burgmayer and Chris Tse for excellent technical support, J. Ecke, Munich for the artwork, and M.L. Gage for editorial comments. Funding support was provided by grants from the Bavarian State Ministry of Sciences, Research and the Arts, *ForNeuroCell* grant (JW), the Federal Ministry of Education and Research 01GN0979, the Mayo Clinic, the Lookout Fund, NIH Grants NIA AG17216 and NINDS NS40256, The Pacific Alzheimer's Research Foundation, Michael J Fox Foundation and the Robert H and Clarice/ML Simpson Foundation Trust Fellowship (HM and MF). BW is a Feodor-Lynen fellow of the Alexander von Humboldt Foundation.

References

Altman J, Das GD. Post-natal origin of microneurones in the rat brain. Nature. 1965; 207:953–956. [PubMed: 5886931]

Babyak M, Blumenthal JA, Herman S, Khatri P, Doraiswamy M, et al. Exercise treatment for major depression: maintenance of therapeutic benefit at 10 months. Psychosom Med. 2000; 62:633–638. [PubMed: 11020092]

Bruel-Jungerman E, Veyrac A, Dufour F, Horwood J, Laroche S, Davis S. Inhibition of PI3K-Akt signaling blocks exercise-mediated enhancement of adult neurogenesis and synaptic plasticity in the dentate gyrus. PLoS One. 2009; 4:e7901. [PubMed: 19936256]

Carballo-Carbajal I, Weber-Endress S, Rovelli G, Chan D, Wolozin B, et al. Leucine-rich repeat kinase 2 induces alpha-synuclein expression via the extracellular signal-regulated kinase pathway. Cell Signal. 2010; 22:821–827. [PubMed: 20074637]

Clelland CD, Barker RA, Watts C. Cell therapy in Huntington disease. Neurosurg Focus. 2008; 24:E9. [PubMed: 18341412]

Cotman CW, Berchtold NC, Christie LA. Exercise builds brain health: key roles of growth factor cascades and inflammation. Trends Neurosci. 2007; 30:464–472. [PubMed: 17765329]

Couillard-Despres S, Winner B, Schaubeck S, Aigner R, Vroemen M, et al. Doublecortin expression levels in adult brain reflect neurogenesis. Eur J Neurosci. 2005; 21:1–14. [PubMed: 15654838]

Crews L, Mizuno H, Desplats P, Rockenstein E, Adame A, et al. Alpha-synuclein alters Notch-1 expression and neurogenesis in mouse embryonic stem cells and in the hippocampus of transgenic mice. J Neurosci. 2008; 28:4250–4260. [PubMed: 18417705]

Curtis MA, Kam M, Nannmark U, Anderson MF, Axell MZ, et al. Human neuroblasts migrate to the olfactory bulb via a lateral ventricular extension. Science. 2007; 315:1243–1249. [PubMed: 17303719]

Eriksson PS, Perfilieva E, Bjork-Eriksson T, Alborn AM, Nordborg C, et al. Neurogenesis in the adult human hippocampus. Nat Med. 1998; 4:1313–1317. [PubMed: 9809557]

Fabel K, Tam B, Kaufer D, Baiker A, Simmons N, et al. VEGF is necessary for exercise-induced adult hippocampal neurogenesis. Eur J Neurosci. 2003; 18:2803–2812. [PubMed: 14656329]

Gloeckner CJ, Schumacher A, Boldt K, Ueffing M. The Parkinson disease-associated protein kinase LRRK2 exhibits MAPKKK activity and phosphorylates MKK3/6 and MKK4/7, in vitro. J Neurochem. 2009; 109:959–968. [PubMed: 19302196]

Gundersen HJ, Bendtsen TF, Korbo L, Marcussen N, Moller A, et al. Some new, simple and efficient stereological methods and their use in pathological research and diagnosis. Apmis. 1988; 96:379–394. [PubMed: 3288247]

Healy DG, Falchi M, O'Sullivan SS, Bonifati V, Durr A, et al. Phenotype, genotype, and worldwide genetic penetrance of LRRK2-associated Parkinson's disease: a case-control study. Lancet Neurol. 2008; 7:583–590. [PubMed: 18539534]

Hoglinger GU, Rizk P, Muriel MP, Duyckaerts C, Oertel WH, et al. Dopamine depletion impairs precursor cell proliferation in Parkinson disease. Nat Neurosci. 2004; 7:726–735. [PubMed: 15195095]

Hsu CH, Chan D, Greggio E, Saha S, Guillily MD, et al. MKK6 binds and regulates expression of Parkinson's disease-related protein LRRK2. J Neurochem. 2010; 112:1593–1604. [PubMed: 20067578]

Hulihan MM, Ishihara-Paul L, Kachergus J, Warren L, Amouri R, et al. LRRK2 Gly2019Ser penetrance in Arab-Berber patients from Tunisia: a case-control genetic study. Lancet Neurol. 2008; 7:591–594. [PubMed: 18539535]

Kempermann G, Chesler EJ, Lu L, Williams RW, Gage FH. Natural variation and genetic covariance in adult hippocampal neurogenesis. Proc Natl Acad Sci U S A. 2006; 103:780–785. [PubMed: 16407118]

Khan NL, Jain S, Lynch JM, Pavese N, Abou-Sleiman P, et al. Mutations in the gene LRRK2 encoding dardarin (PARK8) cause familial Parkinson's disease: clinical, pathological, olfactory and functional imaging and genetic data. Brain. 2005; 128:2786–2796. [PubMed: 16272164]

Kohl Z, Kandasamy M, Winner B, Aigner R, Gross C, et al. Physical activity fails to rescue hippocampal neurogenesis deficits in the R6/2 mouse model of Huntington's disease. Brain Res. 2007; 1155:24–33. [PubMed: 17512917]

Langston JW. The Parkinson's complex: parkinsonism is just the tip of the iceberg. Ann Neurol. 2006; 59:591–596. [PubMed: 16566021]

Lazic SE, Grote HE, Blakemore C, Hannan AJ, van Dellen A, et al. Neurogenesis in the R6/1 transgenic mouse model of Huntington's disease: effects of environmental enrichment. Eur J Neurosci. 2006; 23:1829–1838. [PubMed: 16623840]

Lee H, Melrose HL, Yue M, Pare JF, Farrer MJ, Smith Y. Lrrk2 localization in the primate basal ganglia and thalamus: a light and electron microscopic analysis in monkeys. Exp Neurol. 2010; 224:438–447. [PubMed: 20483355]

Li Y, Liu W, Oo TF, Wang L, Tang Y, et al. Mutant LRRK2(R1441G) BAC transgenic mice recapitulate cardinal features of Parkinson's disease. Nat Neurosci. 2009; 12:826–828. [PubMed: 19503083]

Liou AK, Leak RK, Li L, Zigmond MJ. Wild-type LRRK2 but not its mutant attenuates stress-induced cell death via ERK pathway. Neurobiol Dis. 2008; 32:116–124. [PubMed: 18675914]

MacLeod D, Dowman J, Hammond R, Leete T, Inoue K, Abeliovich A. The familial Parkinsonism gene LRRK2 regulates neurite process morphology. Neuron. 2006; 52:587–593. [PubMed: 17114044]

Marais L, Stein DJ, Daniels WM. Exercise increases BDNF levels in the striatum and decreases depressive-like behavior in chronically stressed rats. Metab Brain Dis. 2009; 24:587–597. [PubMed: 19844781]

Mata IF, Wedemeyer WJ, Farrer MJ, Taylor JP, Gallo KA. LRRK2 in Parkinson's disease: protein domains and functional insights. Trends Neurosci. 2006; 29:286–293. [PubMed: 16616379]

Melrose HL, Daechsel JC, Behrouz B, Lincoln SJ, Yue M, et al. Impaired dopaminergic neurotransmission and microtubule-associated protein tau alterations in human LRRK2 transgenic mice. Neurobiol Dis. 2010

Melrose HL, Kent CB, Taylor JP, Dachsel JC, Hinkle KM, et al. A comparative analysis of leucine-rich repeat kinase 2 (Lrrk2) expression in mouse brain and Lewy body disease. Neuroscience. 2007; 147:1047–1058. [PubMed: 17611037]

Nagahara AH, Merrill DA, Coppola G, Tsukada S, Schroeder BE, et al. Neuroprotective effects of brain-derived neurotrophic factor in rodent and primate models of Alzheimer's disease. Nat Med. 2009; 15:331–337. [PubMed: 19198615]

Naylor AS, Bull C, Nilsson MK, Zhu C, Bjork-Eriksson T, et al. Voluntary running rescues adult hippocampal neurogenesis after irradiation of the young mouse brain. Proc Natl Acad Sci U S A. 2008; 105:14632–14637. [PubMed: 18765809]

Nimchinsky EA, Sabatini BL, Svoboda K. Structure and function of dendritic spines. Annu Rev Physiol. 2002; 64:313–353. [PubMed: 11826272]

Parisiadou L, Xie C, Cho HJ, Lin X, Gu XL, et al. Phosphorylation of ezrin/radixin/moesin proteins by LRRK2 promotes the rearrangement of actin cytoskeleton in neuronal morphogenesis. J Neurosci. 2009; 29:13971–13980. [PubMed: 19890007]

Persson A, Lindwall C, Curtis MA, Kuhn HG. Expression of ezrin radixin moesin proteins in the adult subventricular zone and the rostral migratory stream. Neuroscience. 2010; 167:312–322. [PubMed: 20109539]

Pieper AA, Xie S, Capota E, Estill SJ, Zhong J, et al. Discovery of a proneurogenic, neuroprotective chemical. Cell. 2010; 142:39–51. [PubMed: 20603013]

Plowey ED, Cherra SJ 3rd, Liu YJ, Chu CT. Role of autophagy in G2019S-LRRK2-associated neurite shortening in differentiated SH-SY5Y cells. J Neurochem. 2008; 105:1048–1056. [PubMed: 18182054]

Reetz K, Lencer R, Hagenah JM, Gaser C, Tadic V, et al. Structural changes associated with progression of motor deficits in spinocerebellar ataxia 17. Cerebellum. 2010; 9:210–217. [PubMed: 20016963]

Rodriguez-Oroz MC, Jahanshahi M, Krack P, Litvan I, Macias R, et al. Initial clinical manifestations of Parkinson's disease: features and pathophysiological mechanisms. Lancet Neurol. 2009; 8:1128–1139. [PubMed: 19909911]

Rosas HD, Koroshetz WJ, Chen YI, Skeuse C, Vangel M, et al. Evidence for more widespread cerebral pathology in early HD: an MRI-based morphometric analysis. Neurology. 2003; 60:1615–1620. [PubMed: 12771251]

Sahay A, Hen R. Adult hippocampal neurogenesis in depression. Nat Neurosci. 2007; 10:1110–1115. [PubMed: 17726477]

Sakaguchi-Nakashima A, Meir JY, Jin Y, Matsumoto K, Hisamoto N. LRK-1, a C. elegans PARK8-related kinase, regulates axonal-dendritic polarity of SV proteins. Curr Biol. 2007; 17:592–598. [PubMed: 17346966]

Sala C. Molecular regulation of dendritic spine shape and function. Neurosignals. 2002; 11:213–223. [PubMed: 12393947]

Santarelli L, Saxe M, Gross C, Surget A, Battaglia F, et al. Requirement of hippocampal neurogenesis for the behavioral effects of antidepressants. Science. 2003; 301:805–809. [PubMed: 12907793]

Silveira-Moriyama L, Guedes LC, Kingsbury A, Ayling H, Shaw K, et al. Hyposmia in G2019S LRRK2-related parkinsonism: clinical and pathologic data. Neurology. 2008; 71:1021–1026. [PubMed: 18809839]

Spires TL, Grote HE, Varshney NK, Cordery PM, van Dellen A, et al. Environmental enrichment rescues protein deficits in a mouse model of Huntington's disease, indicating a possible disease mechanism. J Neurosci. 2004; 24:2270–2276. [PubMed: 14999077]

Suominen-Troyer S, Davis KJ, Ismail AH, Salvendy G. Impact of physical fitness on strategy development in decision-making tasks. Percept Mot Skills. 1986; 62:71–77. [PubMed: 3960686]

Tillerson JL, Caudle WM, Reveron ME, Miller GW. Exercise induces behavioral recovery and attenuates neurochemical deficits in rodent models of Parkinson's disease. Neuroscience. 2003; 119:899–911. [PubMed: 12809709]

Tolosa E, Poewe W. Premotor Parkinson disease. Neurology. 2009; 72:S1. [PubMed: 19256022]

van Dellen A, Blakemore C, Deacon R, York D, Hannan AJ. Delaying the onset of Huntington's in mice. Nature. 2000; 404:721–722. [PubMed: 10783874]

van Egmond WN, Kortholt A, Plak K, Bosgraaf L, Bosgraaf S, et al. Intramolecular activation mechanism of the Dictyostelium LRRK2 homolog Roco protein GbpC. J Biol Chem. 2008; 283:30412–30420. [PubMed: 18703517]

van Praag H, Christie BR, Sejnowski TJ, Gage FH. Running enhances neurogenesis, learning, and long-term potentiation in mice. Proc Natl Acad Sci U S A. 1999a; 96:13427–13431. [PubMed: 10557337]

van Praag H, Kempermann G, Gage FH. Running increases cell proliferation and neurogenesis in the adult mouse dentate gyrus. Nat Neurosci. 1999b; 2:266–270. [PubMed: 10195220]

van Praag H, Schinder AF, Christie BR, Toni N, Palmer TD, Gage FH. Functional neurogenesis in the adult hippocampus. Nature. 2002; 415:1030–1034. [PubMed: 11875571]

Wang L, Xie C, Greggio E, Parisiadou L, Shim H, et al. The chaperone activity of heat shock protein 90 is critical for maintaining the stability of leucine-rich repeat kinase 2. J Neurosci. 2008; 28:3384–3391. [PubMed: 18367605]

West AB, Moore DJ, Choi C, Andrabi SA, Li X, et al. Parkinson's disease-associated mutations in LRRK2 link enhanced GTP-binding and kinase activities to neuronal toxicity. Hum Mol Genet. 2007; 16:223–232. [PubMed: 17200152]

Williams RW, Rakic P. Three-dimensional counting: an accurate and direct method to estimate numbers of cells in sectioned material. J Comp Neurol. 1988; 278:344–352. [PubMed: 3216047]

Winner B, Couillard-Despres S, Geyer M, Aigner R, Bogdahn U, et al. Dopaminergic lesion enhances growth factor-induced striatal neuroblast migration. J Neuropathol Exp Neurol. 2008a; 67:105–116. [PubMed: 18219258]

Winner B, Geyer M, Couillard-Despres S, Aigner R, Bogdahn U, et al. Striatal deafferentation increases dopaminergic neurogenesis in the adult olfactory bulb. Exp Neurol. 2006; 197:113–121. [PubMed: 16246330]

Winner B, Lie DC, Rockenstein E, Aigner R, Aigner L, et al. Human wild-type alpha-synuclein impairs neurogenesis. J Neuropathol Exp Neurol. 2004; 63:1155–1166. [PubMed: 15581183]

Winner B, Rockenstein E, Lie DC, Aigner R, Mante M, et al. Mutant alpha-synuclein exacerbates age-related decrease of neurogenesis. Neurobiol Aging. 2008b; 29:913–925. [PubMed: 17275140]

Zhao C, Teng EM, Summers RG Jr, Ming GL, Gage FH. Distinct morphological stages of dentate granule neuron maturation in the adult mouse hippocampus. J Neurosci. 2006; 26:3–11. [PubMed: 16399667]

Zimprich A, Biskup S, Leitner P, Lichtner P, Farrer M, et al. Mutations in LRRK2 cause autosomal-dominant parkinsonism with pleomorphic pathology. Neuron. 2004a; 44:601–607. [PubMed: 15541309]

Zimprich A, Muller-Myhsok B, Farrer M, Leitner P, Sharma M, et al. The PARK8 locus in autosomal dominant parkinsonism: confirmation of linkage and further delineation of the disease-containing interval. Am J Hum Genet. 2004b; 74:11–19. [PubMed: 14691730]

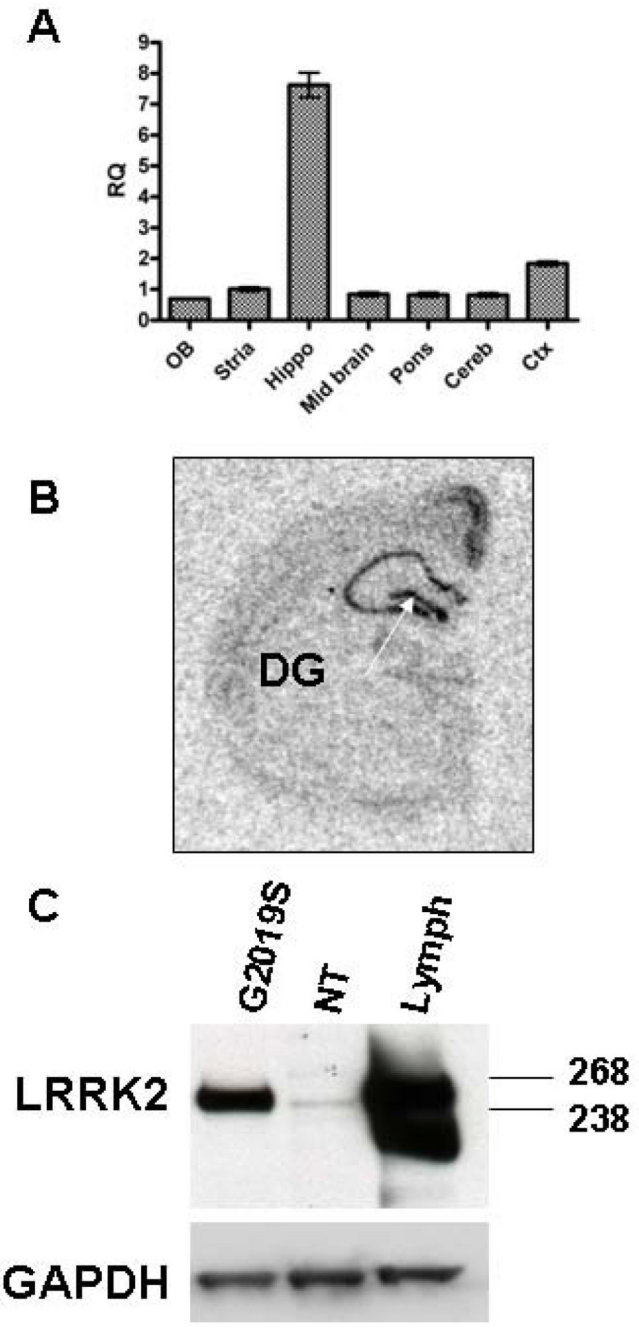

Figure 1. Transgenic human G2019S Lrrk2 is highly expressed in the hippocampus

A: Real time RT-PCR with a human-specific *LRRK2* Taqman probe reveals highest transgene mRNA expression in the hippocampus. B: Finer mapping of transgene expression using i*n situ* hybridization with a human-specific probe confirms high DG (arrow) expression of Lrrk2. C: Immunoblot with a Lrrk2-specific antibody shows robust transgenic human expression.

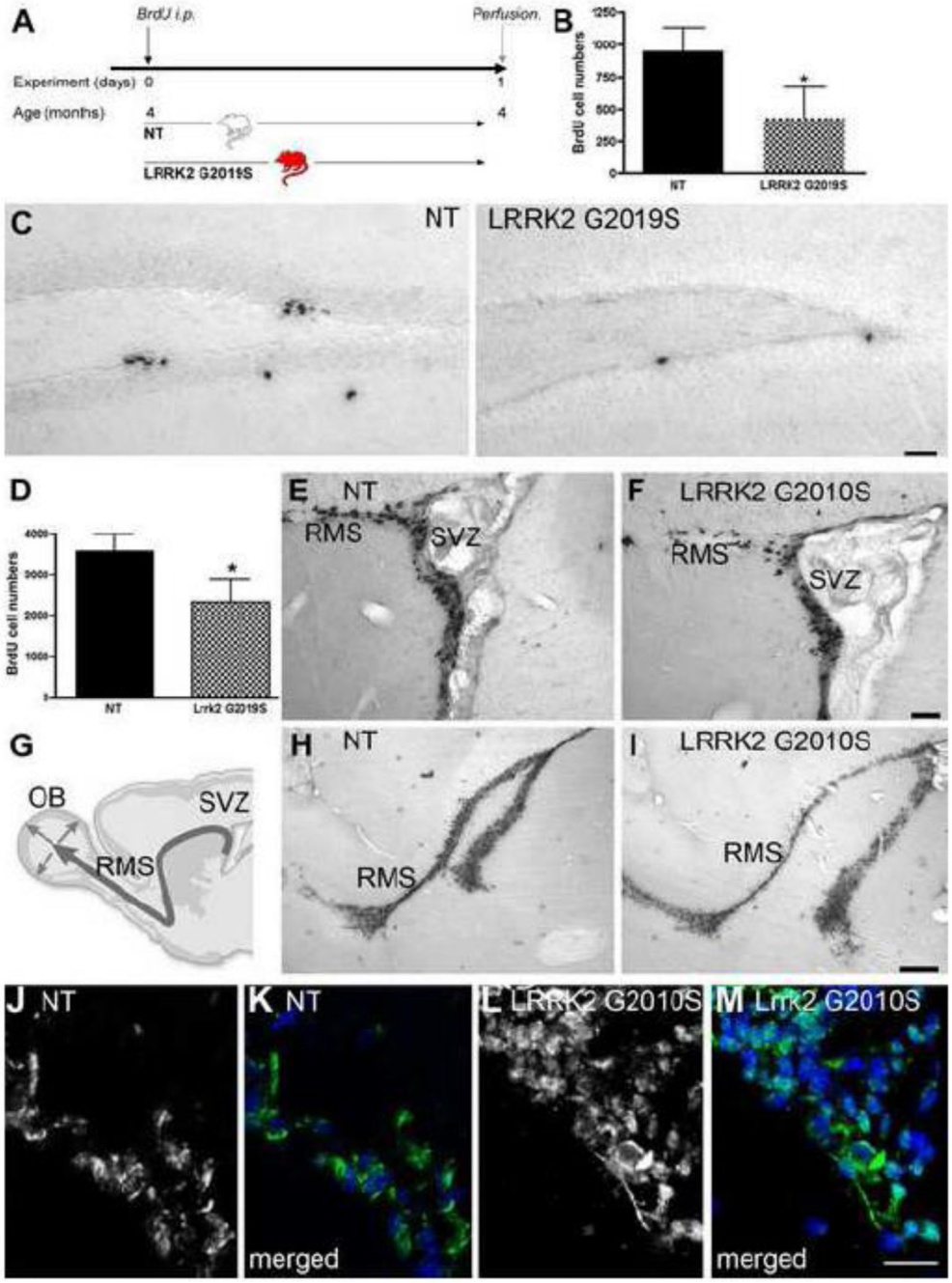

Figure 2. Proliferation is decreased in G2019S transgenic mice

A: Experimental design for the non-transgenic control (NT) and Lrrk2 G2019S mice. Animals were perfused 24 hours after a single BrdU injection (100 mg/kg). B: BrdU cell numbers indicating mitotic cells within the hippocampal DG of the respective groups are decreased in G2019S Lrrk2 transgenic mice; mean number of BrdU-positive cells ± SD, *p<0.01. C: Representative images of DAB staining of BrdU-positive cells in the DG of the different groups, NT: non-transgenic. Scale bar, 50 μm. D–F: Proliferation, presented as the mean number of BrdU-positive cells ± SD, is decreased in the SVZ of G2019S Lrrk2 transgenic mice; E, F show representative images of an overview of the BrdU-positive cells, that are decreased in the SVZ/ RMS of Lrrk2 G2019S mice (F) compared to NT (E). Scale

bar in E, F, 50 μm. G: Schematic drawing of the SVZ/olfactory bulb (OB) system. H, I: A thinner stream of newly generated cells (BrdU-positive) is present in the rostral migratory stream (RMS) of Lrrk2 G2019S mice (I) compared to controls (H), Scale bar, 250 μm. Expression of LRRK2 is observed in the SVZ of NT mice (J, Lrrk2 in green merged with Dapi, blue in K) and more strongly in the SVZ of LRRK2 G2019S mice (L, Lrrk2 in green merged with Dapi, blue in M). Scale bar, 20 μm (E, F, H, I).

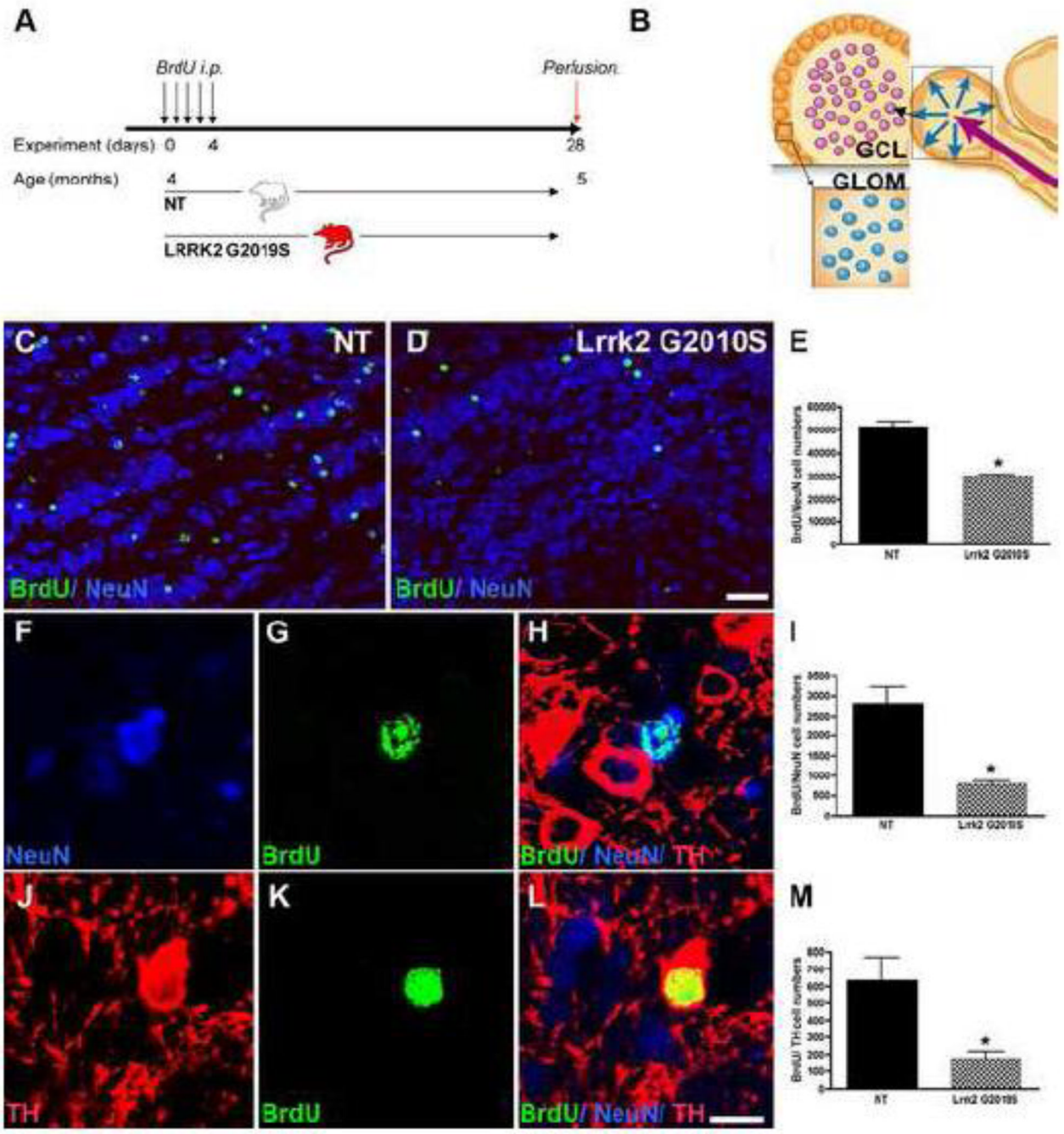

Figure 3. Olfactory neurogenesis is decreased in G2010S transgenic mice

A: Experimental design for the non-transgenic control (NT) and Lrrk2 G2019S mice. Animals received BrdU injections (50 mg/kg) on five consecutive days and were perfused one month after the BrdU injections. B: Schematic overview of the two neurogenic regions of the olfactory bulb analyzed, the granule cell layer (GCL) and the glomerular layer (GLOM). C–E: Analysis of neurogenesis in the GCL in NT (C) and Lrrk2 G2010S mice (D) reveals a significant decrease in BrdU/NeuN-positive cells in the transgenic mice (E, *p<0.01). BrdU-positive cells are depicted in green in C, D; NeuN-positive cells are in blue in C, D. (Scale bar in C, D, 25 μm). F–M: Analysis of neurogenesis in the GLOM. Neurogenesis (I) and dopaminergic neurogenesis (M) are both decreased in transgenic mice

(*p<0.01). F–H: examples of newly generated neurons (BrdU/NeuN) and J–L: examples of newly generated dopaminergic neurons (BrdU/TH, Scale bars F–H and J–L, 10 μm). BrdU is depicted in green, TH is depicted in red and NeuN is depicted in green.

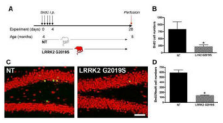

Figure 4. Fewer new neurons survive in G2019S transgenic mice

A: Experimental design for the non-transgenic control (NT) and Lrrk2 G2019S mice. B: Cell numbers of newly generated cells (BrdU-positive) in the hippocampal DG from the respective groups are presented as the mean number of BrdU-positive cells ± SD, *p<0.01. C: Representative images of BrdU-positive cells (green) colabeled with NeuN (red) for the groups indicated. Scale bar, 50 μm. D: Cell numbers of newly generated neurons (BrdU/NeuN-positive) in the DG, *p<0.0.01, compared to NT.

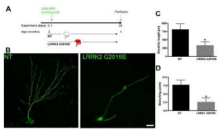

Figure 5. Defects in dendrite outgrowth of new neurons in G2019S transgenic mice

A: Experimental design for the non-transgenic control (NT) and Lrrk2 G2019S mice. Animals were stereotactically injected with CAG-GFP retrovirus and were perfused one month later. B: Representative images of GFP-positive cells in the DG of NT and Lrrk2 G2019S mice. Scale bar, 20 μm. Quantitative analysis for dendrite length (C) and branching points (D), ± SD, *p<0.01.

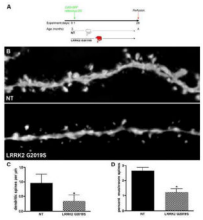

Figure 6. Spine number and maturation are decreased in G2019S transgenic mice

A: Experimental design for the non-transgenic control (NT) and Lrrk2 G2019S mice. Animals were stereotactically injected with CAG-GFP retrovirus and were perfused one month later. B: Representative images of GFP-positive dendrites in the DG of NT and Lrrk2 G2019S mice. Scale bar, 5 μm. Quantitative analysis for C: dendritic spines/μm and D: percentage of mushroom spines, * $p<0.001$.

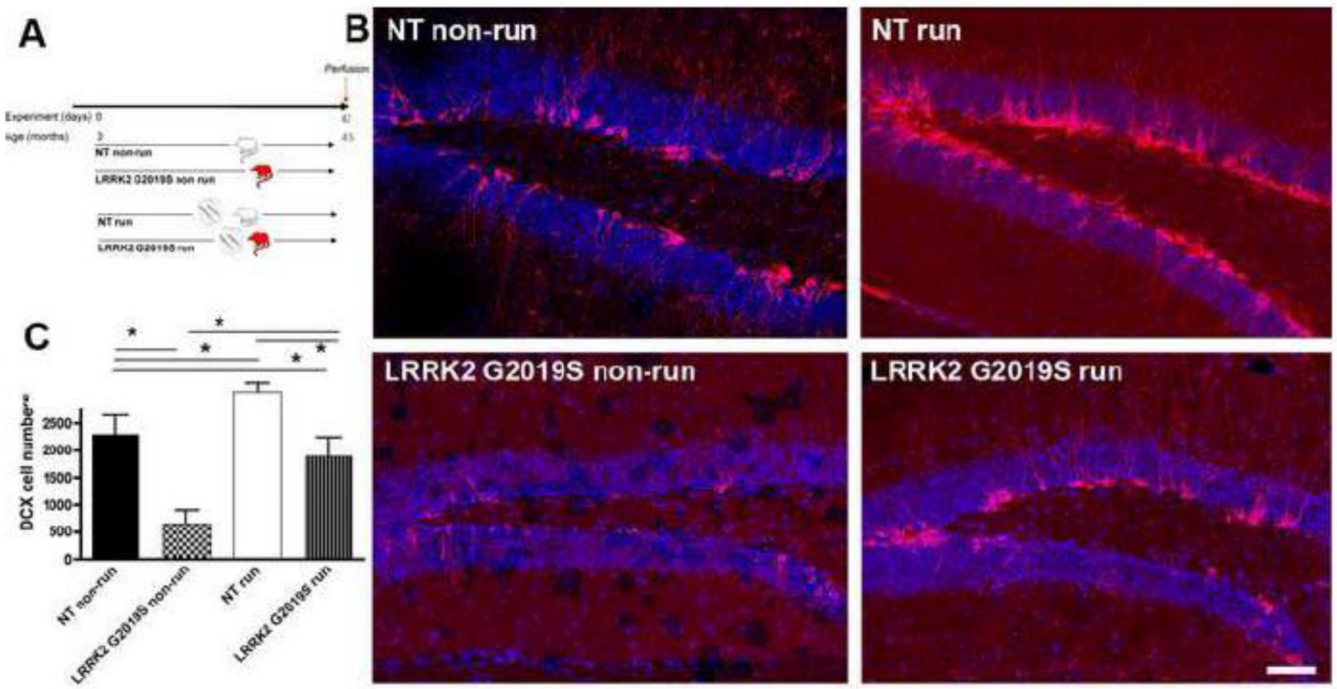

Figure 7. Running partly reverses negative impact of G2019S on neurogenesis

A: Experimental design for the non-transgenic control (NT) and Lrrk2 G2019S mice, running (run) or non-running (non-run). B: Representative images of DCX-positive neuroblasts in the DG of NT and Lrrk2 G2019S mice (red: DCX, blue: NeuN). Note the increase in numbers of DCX-positive cells after running. C: Quantitative analysis for the total number of DCX-positive cells in the DG. Scale bar, 50 μm, * $p<0.05$.